Effect of Crystallization Conditions on Spherulitic Texture and Tensile Properties of sPS/PPO Blends

G. Dutt, K. M. Kit

Department of Materials Science and Engineering, University of Tennessee, Knoxville, Tennessee 37996-2200

Received 20 August 2001; accepted 18 October 2001

ABSTRACT: In the second study on melt-miscible syndiotactic polystyrene (sPS) and poly(phenylene oxide) (PPO) blends, the effect of processing conditions on morphology, ultimate tensile properties, and the mode of fracture is reported. Bulk samples of the blends were molded and then crystallized from melt as well as from the quenched state at different temperatures. The spherulitic morphology of the melt-crystallized blends, observed by scanning electron microscopy, revealed formation of complete, well-developed spherulites whose texture increased in coarseness with increasing crystallization temperatures. In all the cold-crystallized blends lamellar bundles formed a meshlike structure whose texture did not vary significantly with crystallization temperature. Depending on the crystallization temperature, 50/50 melt-crystallized blends showed varying tensile properties and different modes of failure. In the samples with the largest amorphous domain size of 0.6 μm, the amorphous ellipsoids were cold drawn into fibrils during tensile loading and very high tensile strengths were recorded. The tensile properties for the other melt-crystallized and all cold-crystallized blends did not vary substantially with the changing crystallization temperature. The micrographs of the fractured surfaces of the melt-crystallized blends suggested that, although intraspherulitic fracture occurred at low crystallization temperatures, interspherulitic fracture took place at high crystallization temperatures. The correlation of the morphology and mechanical properties suggests that melt-miscible blends have good interfacial adhesion between phases and that, by varying composition and processing conditions, it might be possible to control amorphous domain sizes, which is critical in achieving better mechanical properties. © 2003 Wiley Periodicals, Inc. J Appl Polym Sci 87: 1984–1994, 2003

Key words: syndiotactic polystyrene; poly(phenylene oxide); crystallization; spherulitic morphology; tensile strength

INTRODUCTION

Increasing the toughness of engineering polymers by promoting energy-absorbing mechanisms such as stretching-tearing, crazing, yielding, or some combination of these has been the focus of extensive research. The most common method used is rubber toughening, which involves addition and control of an immiscible, discontinuous elastomeric phase. Examples include polystyrene (PS),[1] poly(styrene–acrylonitrile) copolymer (SAN),[2] polyamide 6 (PA),[3] and poly(methyl methacrylate) (PMMA).[4] In these materials the underlying mechanisms of energy absorption involved are fairly well understood.

Another approach consists of incorporation of rigid thermoplastic particles to the rigid matrix. One advantage of this methodology is that little or no reduction in stiffness is usually observed. The energy absorption mechanisms of interfacial bonding, massive crazing, shear yielding, and cold drawing have been identified with these blends.[5–8] An order of magnitude increase in the impact strength of isotactic polypropylene (iPP) was seen in a blend with 10% Noryl (aPS/PPO blend) and 2% of a block copolymer compatibilizer.[9] Neat Noryl is stiffer and more brittle than iPP, but when present as small particles ($\sim$ 0.8 μm), it induced massive crazing and shear yielding in the iPP matrix. Noryl particles of 0.3 and 10 μm were shown to be less effective in increasing the toughness of iPP. When polycarbonate (PC) was blended with styrene–acrylonitrile (SAN), increases in stiffness, yield strength, strain at failure, and toughness were observed.[10] Although neat SAN is brittle with a strain at failure of just 5%, 1 μm SAN particles in 10% SAN blends elongated an average of 100% in tensile specimens that were tested to failure. This behavior was most likely responsible for the increases in ductility and toughness of the PC. The large plastic deformation of SAN particles was attributed to large compressive stresses ($\sim$ 2–8 MPa) exerted on the particles under tensile loading resulting from the stiffness mismatch between SAN and PC. PMMA particles in polycarbonate matrix have also been shown to undergo plastic deformation, resulting in improved yield strength, elongation, and in some cases even toughness.[11] Again, particle size was crucial in inducing the brittle–ductile transformation in the brittle PMMA particles. Other examples of the rigid particle toughening systems in-

Correspondence to: K. Kit (kkit@utk.edu).

Contract grant sponsor: DuPont Educational Aid Program.

Journal of Applied Polymer Science, Vol. 87, 1984–1994 (2003)

clude iPP/poly(ethylene terephthalate)[12] and poly(butylene terephthalate)/SAN.[11]

The effect of morphology of semicrystalline rigid–rigid blends on the deformation mechanisms has not been addressed. Semicrystalline polymers, under certain conditions, develop textures consisting of bundles.[13–16] Amorphous regions of the same scale separate these bundles. The amorphous material, having different composition and modulus, might also be trapped in other asymmetric regions formed by branching and splaying of the lamellae. In melt-miscible blends, the interfacial strength between these regions can be expected to be very high because of entanglement of the chains in the amorphous phase with loops and tie chains, and incorporation of the chain ends in the lamellar crystals. At certain crystallization condition and blend composition, the amorphous phase composition may result in these amorphous phases acting as toughenners. In that event, it can be reasonably hoped that significant energy-absorbing deformation process may occur.

The main objective of the present work is to understand the effect of spherulitic texture of melt-miscible, rigid–rigid semicrystalline syndiotactic polystyrene (sPS) and poly(phenylene oxide) (PPO) blends on their mechanical properties. It has been shown by us[17] that sPS and PPO are completely melt miscible over the composition range being studied. As sPS crystallizes from the melt, PPO is rejected from the crystalline phase and a two-phase system results: (1) a crystalline phase containing 100% sPS and (2) an amorphous phase containing sPS and PPO but enriched in PPO compared to the overall blend composition. This PPO-enriched amorphous phase may then act as a toughening phase similar to Noryl in iPP[9] or SAN in PC.[10] In this work, the blends were subjected to different processing conditions to produce different levels of segregation of PPO during crystallization. The resulting texture and morphology were correlated to the tensile properties of the bulk samples.

EXPERIMENTAL

Syndiotactic polystyrene used for this study was kindly provided by Dow Chemical Company (Questra LA320; Midland, MI). The poly(phenylene oxide) (PPO) was purchased from Scientific Polymer Products (Ontario, NY). For this work, two sPS/PPO compositions (50/50 and 67/33) were melt blended. These were designated as sPS50PPO and sPS67PPO, respectively (the middle digits represent the weight percentage of the sPS in the blend). The materials and the procedure for melt blending were described in detail in a previous study.[17]

Molding and crystallization of bulk samples

Dog bone–shape bulk samples of sPS50PPO and sPS67PPO blends were molded in an Atlas mixing molder (Chicago, IL) for mechanical testing. The mold conformed to the ASTM 1708-B standard. The mixing cup temperature was kept at 304°C, and the mold was heated to approximately 240°C. After the injection, the mold was taken out of the clamp and quenched in water. For mechanical testing of the pure sPS, neat sPS was compression molded into 1-mm-thick sheets in a rectangular 125 × 150 mm aluminum frame.

The bulk samples were crystallized from the melt as well as the quenched state. The Wabash hot press (Wabash, IN) used for crystallization was calibrated in atactic polystyrene (aPS) melt by use of an external thermocouple.

The as-molded samples were put in an aluminum frame, designed for holding the dog bone–shape samples, and melted in a furnace. The samples to be cold crystallized were immediately quenched in an ice bath and then transferred to the preheated hot press. The cold crystallization temperatures were 180, 190, and 220°C. For melt crystallization, the samples from the furnace were transferred directly to the hot press preheated to the crystallization temperature. Melt crystallization was done at 220, 245, and 255°C.

Injection-molded samples of neat sPS could not be crystallized in the dog bone–shape aluminum frame because of their brittleness. Therefore, the neat sPS sheets, compression molded in the rectangular frame, were subjected to the same melting and crystallization treatment. Dog bone–shape samples conforming to ASTM D-638 (type M-II) standard were machined from these rectangular sheets.

Tensile testing

All tensile testing was done on a Thwing-Albert EJA-2000 tensile tester (Philadelphia, PA). Dog bone–shape samples of the crystallized blends (ASTM 1708-95) were tested at a crosshead speed of 1 mm/min. Crystallized neat sPS samples [ASTM D-638 (M-II)] were tested at a crosshead speed of 5.0 mm/min. In all the tests the strain rate was 6.67×10^{-4} s^{-1}. At least five samples of each composition and crystallization temperature were tested.

Scanning Electron Microscopy

The dog bone–shape tensile testing samples and fracture surfaces were sequentially etched in 66 and 33% solutions of 1,2-dichlorobenzene in amyl acetate, at room temperature, in an ultrasonic bath for 35 s each. These were then rinsed in amyl acetate to avoid the precipitation of sPS. Finally, the films were washed in methanol, rinsed in water, and dried. This etching

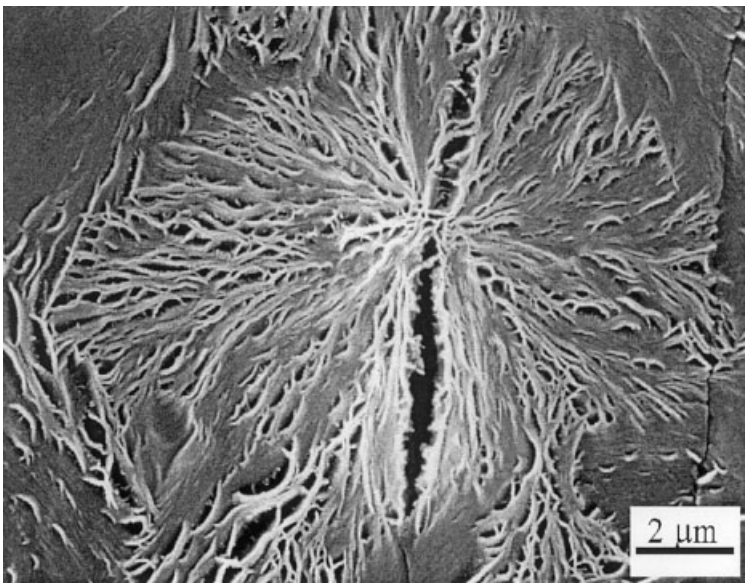

Figure 1 sPS50PPO melt crystallized at 220°C.

process dissolved the amorphous material in the crystallized blend samples and provided the contrast for the observation of the crystalline bundles. The removed amorphous regions appeared as voids in the SEM micrographs. All samples were mounted on a stub and sputtered with gold in a Technics Hummer I sputter (Munich, Germany) before observation. The specimens were observed in a Cambridge electron microscope (Oxford Instruments, Oxford, MI) and a Hitachi S-3000N (Hitachi, Tokyo, Japan) electron microscope. In both the microscopes an accelerating voltage of 15 kV was used. The Scion Image program was used for making the bundle thickness and spacing measurements from the SEM micrographs. At least 50 measurements of a particular feature were made from the micrograph and the average values were reported.

RESULTS AND DISCUSSION

Scanning electron microscopy

Melt-crystallized blends

SEM micrographs of etched sPS50PPO, melt crystallized at 220, 245, and 255°C, are shown in Figures 1 through 3, respectively. The micrograph of etched sPS67PPO blend melt crystallized at 245°C is shown in Figure 4. All these micrographs were taken at 7000× magnification. The etched samples of neat melt-crys-

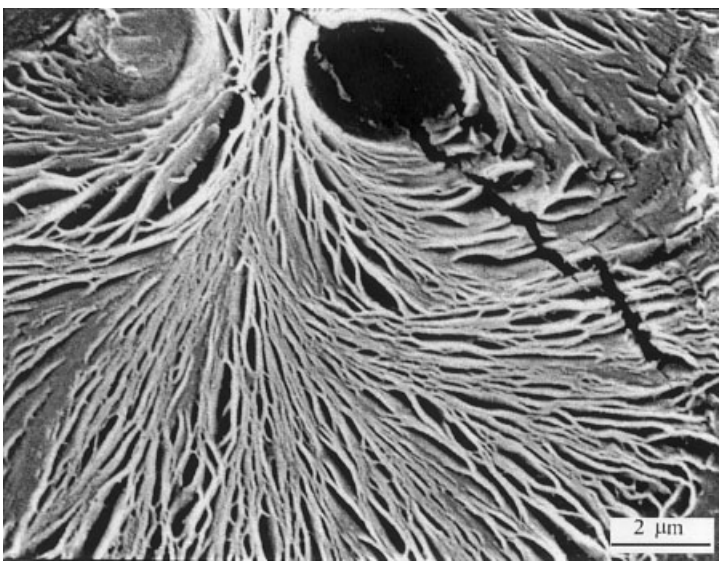

Figure 2 sPS50PPO melt crystallized at 245°C.

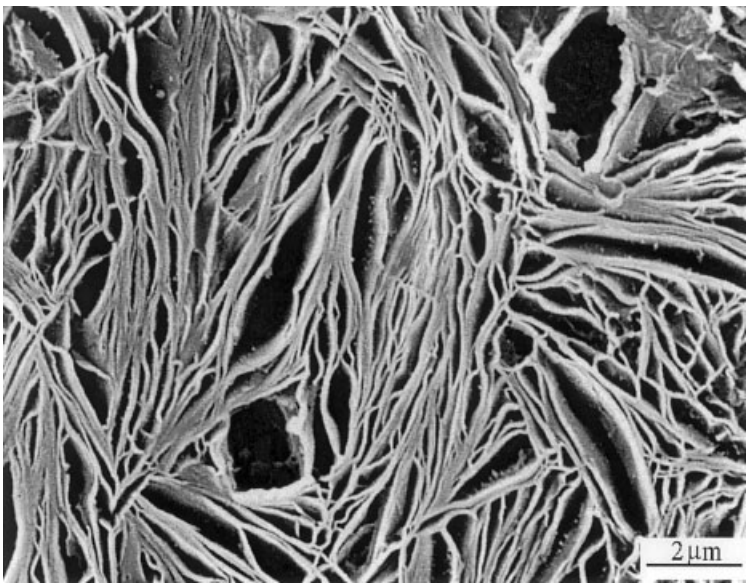

Figure 3 sPS50PPO melt crystallized at 255°C.

tallized sPS did not reveal any features in the SEM. These micrographs show complete or partial sections of etched spherulites. These spherulitic sections consist of ribbonlike fibrous units radiating from a center. These ribbonlike structures, known as *bundles*, are stacks of 5–50 lamellae, as seen from the thickness dimension. Isolated bundles, whose lateral dimensions can be easily measured, are seen at the periphery of the spherulites. The spaces between these crystalline bundles are amorphous regions of the same order of thickness. As these bundles move away from the center, they branch and splay continuously to form ellipsoidal interfibrillar regions, which contain amorphous material. The size of these ellipsoidal regions increases from the center to the periphery of the spherulite.

The variation in the dimensions of the ellipsoidal dimensions and the amorphous interbundle spacings at the corresponding crystallization temperatures is also plotted in Figure 5. *Coarseness* is the measure of absolute size of these bundles and increases with increasing crystallization temperature (lower supercoolings and slower crystallization). This coarseness, however, varies little for different composition blends crystallized at the same temperature. The theory of spherulitic crystallization of Keith and Padden[16] suggests that the change in the bundle thickness with the change in crystallization temperature can be qualita-

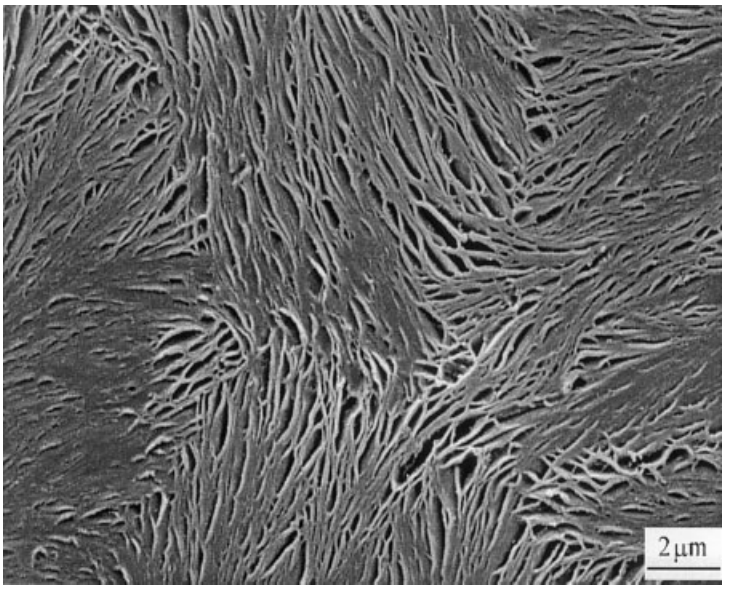

Figure 4 SEM micrograph of sPS67PPO blend melt crystallized at 245°C.

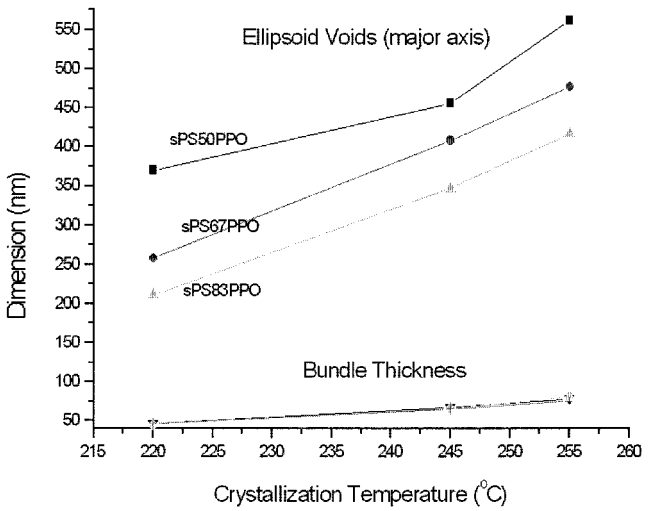

Figure 5 Spherulitic texture measurements on melt-crystallized blends.

tively correlated to the diffusion length δ, which is the ratio of diffusion rate of the rejected species *D* to the crystalline growth rate *G*. At temperatures close to the melting point (e.g., 255 and 245°C), the crystal growth rate *G* is very small and the corresponding diffusion coefficient *D* is very large. Both these factors result in a large value of δ and hence, large bundle thickness. Quantitative predictions of bundle thickness based on finite element simulations of bundle formation and growth in the presence of diluents were carried out by Kit and Schultz.[13] These results also agree with the qualitative relationships proposed by Keith and Padden. When the crystallization temperature is reduced to 220°C, there is a large decrease in the diffusion coefficient *D*, whereas the crystalline growth rate *G*, for the sPS50PPO blend, increases by at least an order of magnitude.[18] The result is a much smaller diffusion length δ and is reflected in the smaller measured bundle thickness.

The thickness of amorphous interbundle regions increases with slower crystallization rate and higher diffusion coefficient at increasing crystallization temperatures. Higher PPO concentration also increases the thickness of these amorphous regions. The dimensions of the ellipsoidal voids (both major and minor axes) also follow the same trend. Compactness does not seem to vary much with change in crystallization temperature for sPS50PPO blends, but with decreasing PPO concentration it increases slightly with increasing crystallization temperature. All these observations can be related to the retarding effect of PPO on crystallization of the sPS. WAXD results in the previous study[17] show that the actual weight percentage of the sPS crystallized (calculated on the basis of weight fraction of sPS in the blend) decreases continuously with increasing PPO content.

Cold-crystallized blends

A SEM micrograph of etched sPS50PPO, cold crystallized at 220°C, is shown in Figure 6. The micrographs for other crystallization temperatures (not shown here) also show a similar meshlike structure of lamellar bundles. The holes in the mesh may either be regions between the small spherulites or amorphous regions formed after branching of the bundles. No complete or identifiable sections of spherulites are seen. The measurement of texture features of these cold-crystallized blends is not possible. The formation of this imperfect structure can be attributed to the quenching step in the processing of these blends. A

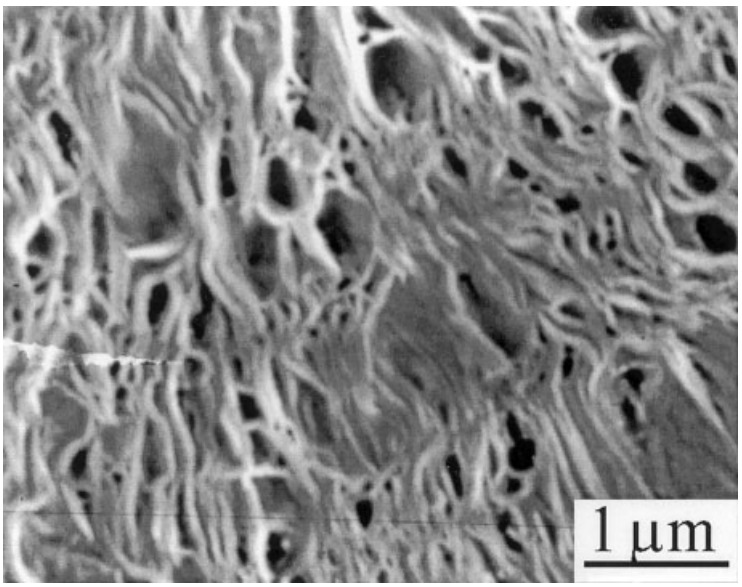

Figure 6 sPS50PPO cold crystallized at 220°C.

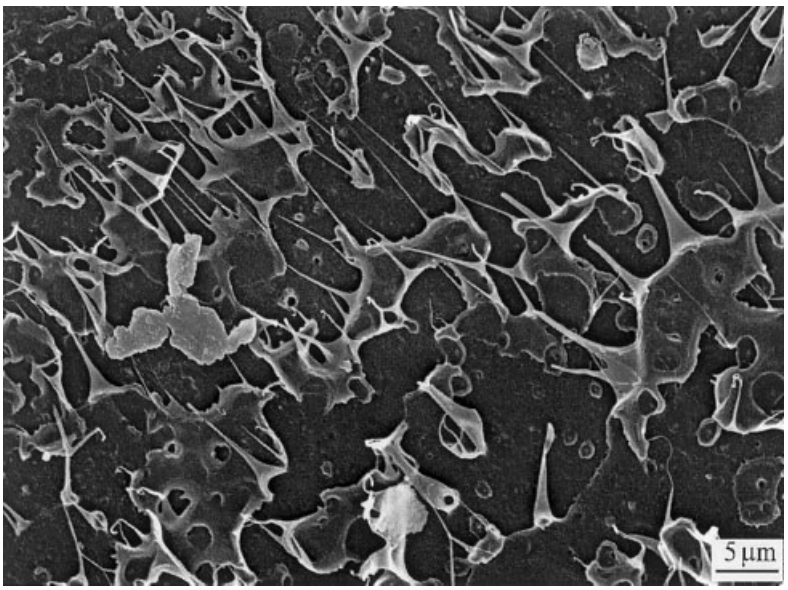

Figure 7 Nonetched fracture surface of sPS50PPO (melt crystallized at 255°C) showing highly drawn fibrils.

sharp drop in the temperature from the melt state to room temperature (below the glass-transition temperature of the blend) and further annealing at high supercoolings result in the formation of a large number of nuclei. These nuclei are almost contiguous to each other. When the blend is crystallized, small, imperfect spherulites are formed that impinge very quickly, resulting in a meshlike structure. Longer annealing times cause secondary crystallization, although there is little change in morphology.

Fracture surfaces

The tensile fracture surfaces of the melt-crystallized sPS50PPO blends, crystallized at 220 and 255°C, were also observed under the SEM. Figure 7 shows the nonetched fracture surface of the sPS50PPO sample melt crystallized at 255°C. The micrograph shows highly elongated fibrils drawn out from the fractured surface. No voids or pits are seen and the surface appears to be quite flat. Because the distance between these fibrils is much smaller than the average diameter of a spherulite ($\sim$ 30 μm), these must be cold-drawn regions within the spherulite. The fracture surface was then etched and the spherulitic morphology revealed is shown in a low magnification micrograph in Figure 8. The uneven surface shows spherulites protruding out of the matrix. The depressed regions are the impressions of the spherulites pulled out from the fracture surface with the other section of the tensile spec-

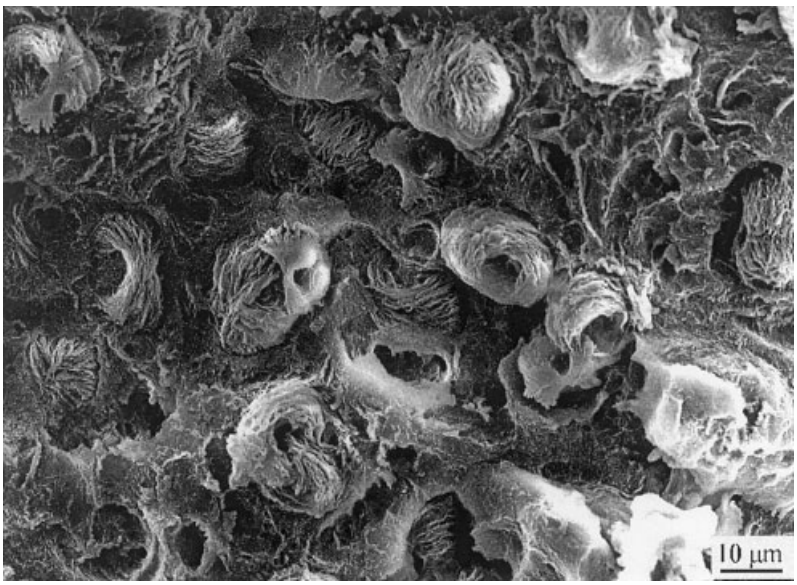

Figure 8 Etched fracture surface of sPS50PPO (melt crystallized at 255°C) showing interspherulitic fracture.

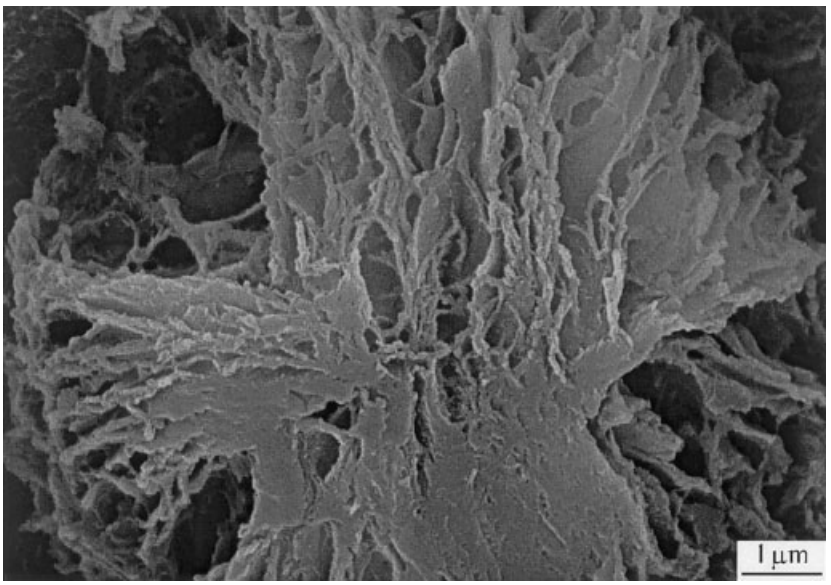

Figure 9 Etched fracture surface of sPS50PPO (melt crystallized at 255°C) showing deformed amorphous regions.

imen. These features indicate an interspherulitic mode of fracture. One spherulite of the same sample imaged at high magnification is shown in Figure 9. The high magnification micrograph of the spherulite suggests that it was also subjected to localized strain. The bundles appear relaxed after the release of the strain. The voids, which consisted of the amorphous material before etching, appear to have undergone deformation and at some points joined with each other to form larger irregular domains. The shape and size of these deformed amorphous regions match closely with the regions from which fibrils were drawn in the nonetched fracture surface. Still, the spherulite did not crack internally and was preserved as a complete structure. Although the test sample failed at the boundaries of the spherulites (interspherulitic fracture), it was accompanied by the drawing of the sPS-rich interfibrillar amorphous domains.

The nonetched fracture surface of the sPS50PPO sample, melt crystallized at 220°C, is shown at the same magnification in Figure 10. In this figure, protruding pyramid-like structures with pointed ridges surrounding pits of various depths can be seen. These pits appear to be formed by the pulling out of parts of the spherulite, resulting in an uneven surface. Chu and Schultz[19] also observed similar structures in poly(ether ether ketone) (PEEK). They suggested that these elevated features are high-density nuclei that remain

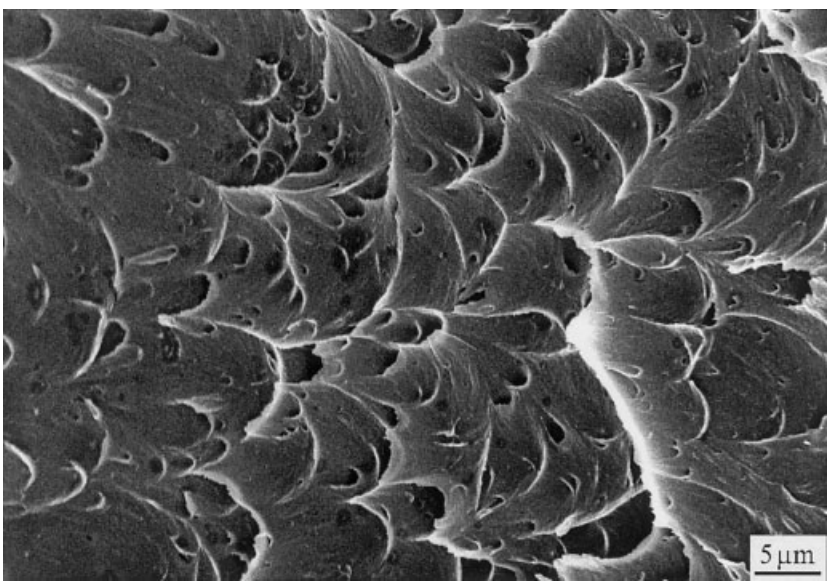

Figure 10 Nonetched fracture surface of sPS50PPO (melt crystallized at 220°C) showing intraspherulitic fracture.

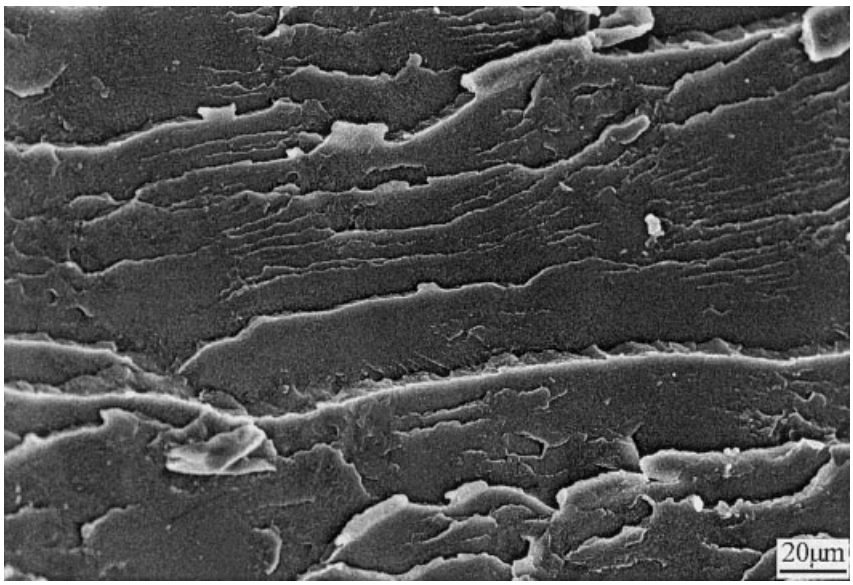

Figure 11 Nonetched fracture surface of neat sPS (melt crystallized at 255°C) showing multilayered microcracks.

after cracking of the spherulite under strain. This intraspherulitic fracture observed can be related to the spherulite density. The density of a spherulite increases from a low-density periphery to a high-density and high-crystallinity nucleus at the center. This density gradient, steeper in smaller spherulites, can lead to propagation of the crack through the spherulite. The fracture surface after etching consisted of etched spherulites impinged with each other, very similar to those seen in the nonfractured films imaged before (Figs. 1–3). This structure suggests that, although the strain did crack the spherulite, the alternating crystalline and amorphous regions forming the bundle were not deformed.

The fracture surfaces of the melt-crystallized blends were also compared to the similar surfaces for the neat sPS. The fractured surface of neat sPS, melt crystallized at 255°C (Fig. 11), consists of several layers of microcracks and voids. This type of structure, formed from a multistep fracture process occurring at different points (because of uneven stress points on the surface), strongly suggests craze growth. The fracture surface of neat sPS, melt crystallized at 220°C (Fig. 12), consists of a structure very similar to the one observed in blends crystallized at 220°C. The spherulitic nuclei at the crack surface are evident from the uneven pyramidal structures coming out of the matrix. Although etched surfaces of the neat sPS do not reveal any

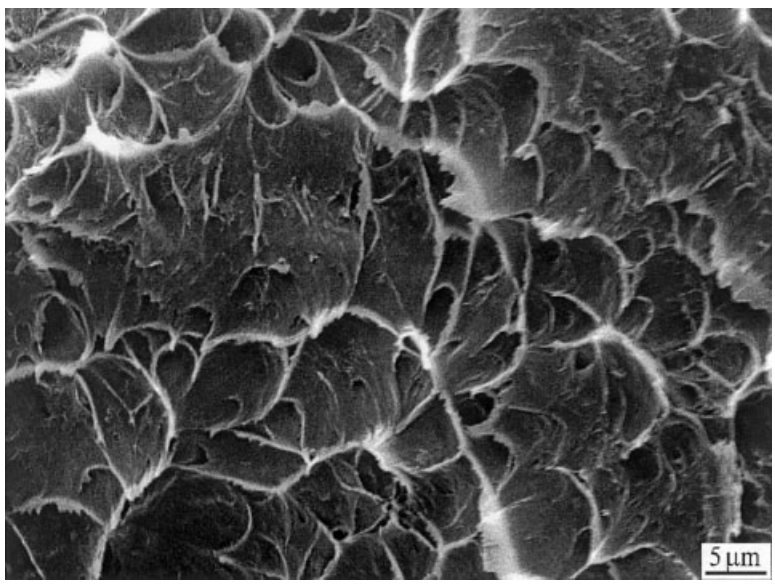

Figure 12 SEM micrograph of nonetched fracture of neat sPS (melt crystallized at 220°C) showing nucleus intraspherulitic fracture.

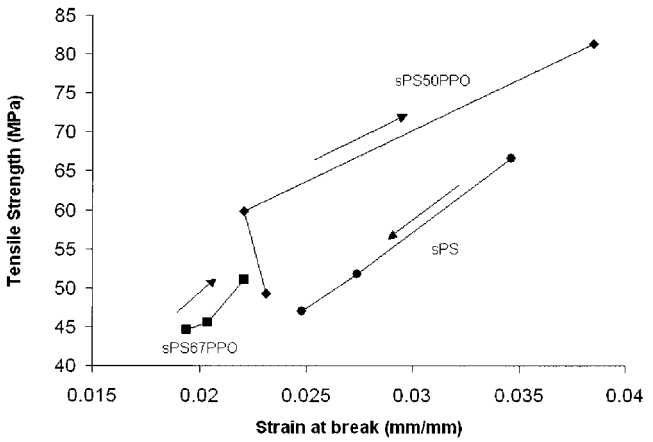

Figure 13 Tensile strength and strain at break for melt-crystallized neat sPS, sPS50PPO, and sPS67PPO. Arrows indicate crystallization temperature increasing from 220 to 245 to 255°C.

spherulitic structures, these features do suggest that intraspherulitic fracture might be taking place in the sPS melt crystallized at 220°C.

Tensile testing

Melt-crystallized blends

The average tensile strength and strain at break for the melt-crystallized sPS, sPS50PPO, and sPS67PPO for different crystallization temperatures are shown in Figure 13. The tensile strength and failure strain values depend largely on PPO content in the blends. For sPS50PPO, the tensile strength increases with crystallization temperature (slower crystallization). A similar, though less pronounced, trend is observed for sPS67PPO. Neat melt-crystallized sPS shows mechanical behavior opposite to that of the melt-crystallized blends. The sample crystallized at 220°C has the highest tensile strength and strain at break. These values decrease with increasing crystallization temperature and decreasing crystallization rate. Although the neat sPS samples were processed slightly differently (compression-molded) than were the blend samples (injection-molded), it is unlikely that this affected the resultant mechanical properties because the melting of the samples in a furnace before isothermal crystallization would have destroyed any thermomechanical history imposed by the molding process. The typical engineering stress–strain curves for the melt-crystallized sPS50PPO blend and melt-crystallized neat sPS are shown in Figure 14(a) and (b). The sPS stress–strain curves are almost linear, whereas those for the blend show a slight convex curvature.

Cold-crystallized blends

The tensile strength and strain at break for cold-crystallized neat sPS, sPS50PPO, and sPS67PPO are shown in Figure 15. Again, the ultimate tensile properties improve with increasing PPO content, but variation with crystallization temperature is essentially minor. At best, these properties are a very weak function of the crystallization temperature. For neat sPS, almost no variation is observed.

Effect of spherulitic texture on tensile properties

The SEM images show that crystallization of the sPS/PPO blends from melt and quenched state resulted in vastly different spherulitic morphologies. The variation in texture with the crystallization temperature was more pronounced in melt-crystallized blends. The tensile testing results suggest that, although tensile strength was a strong function of the initial blend composition, at 50% PPO concentration the tensile properties did vary substantially with the crystallization temperature in melt-crystallized blends. Slower crystallization resulted in coarser bundles and larger amorphous domains as well as higher crystallinity,

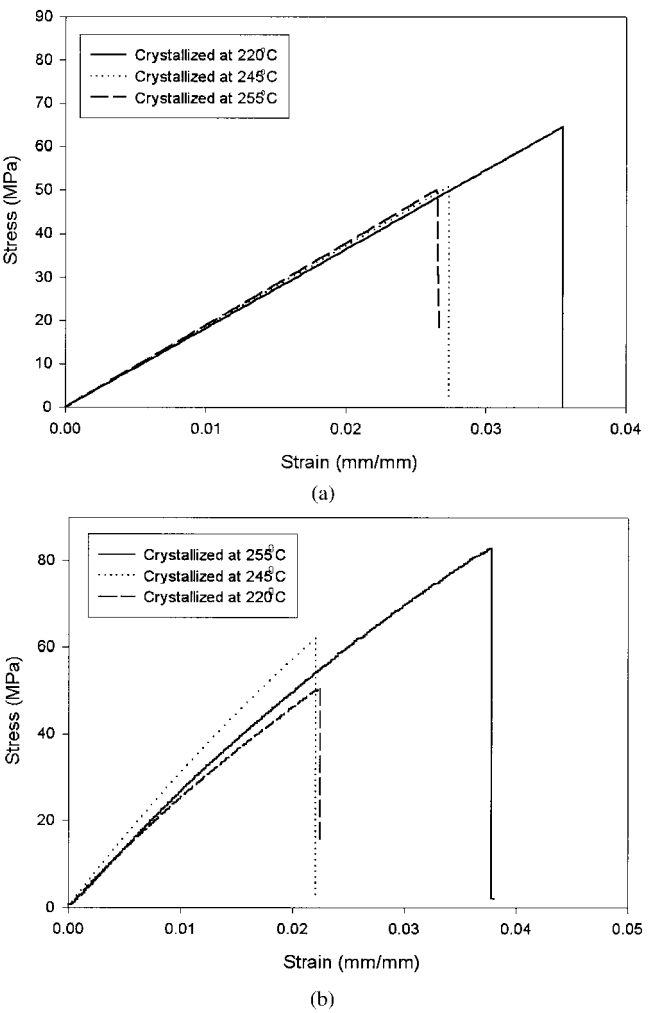

Figure 14 Typical stress–strain curves for (a) melt-crystallized neat sPS and (b) melt-crystallized sPS50PPO.

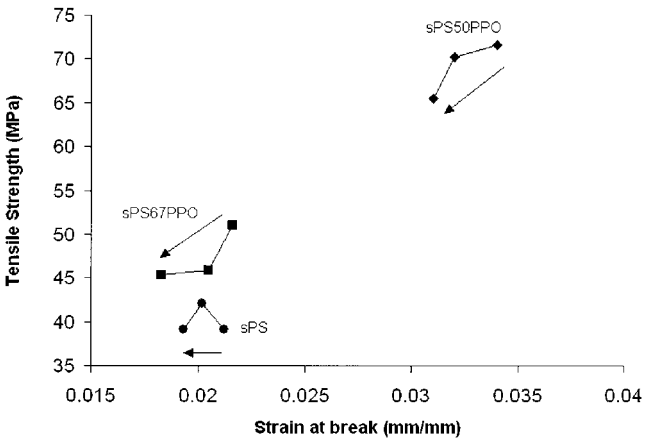

Figure 15 Tensile strength and strain at break for cold-crystallized neat sPS, sPS50PPO, and sPS67PPO. Arrows indicate crystallization temperature increasing from 180 to 190 to 220°C.

and was accompanied by higher tensile strength and strain at break.

The trend in mechanical properties was opposite to the one observed for neat, crystallized sPS samples having higher bulk weight crystallinity. Slowly crystallized, neat sPS samples showed poor mechanical properties, whereas the slow crystallized blends showed better tensile strength, strain at break, and tensile toughness. The enhanced mechanical properties of sPS/PPO melt crystallized slowly cannot be attributed to composition of the amorphous phase domains either. Phase compositions of sPS50PPO melt crystallized at 255°C are quite similar to that of sPS67PPO cold crystallized at 190°C,[17] but the synergistic increase in the tensile strength is not observed in the latter. The trend in tensile strength seems to correlate better with the size of the amorphous domains, with the samples with larger amorphous domains exhibiting higher tensile strength. Control of particle domain sizes and interfacial adhesion between the phases has been recognized to be critical in achieving toughening.[20–22] An optimum particle size range has been found in rigid–rigid blend systems of PA/PPO[5] and compatibilized iPP/Noryl [iPP] blends to relieve the triaxial stress and enable combinations of crazing and shear yielding processes to occur. Rigid PMMA and acrylonitrile–styrene (AS) particles in ductile polycarbonate matrix were also found to undergo plastic deformation under compressive stresses when their diameters were around 1 μm.[11] The amorphous ellipsoids of major dimension 0.6 μm in melt-crystallized sPS50PPO blends were highly drawn before interspherulitic fracture. There was no evidence of failure along the interfaces between the crystalline bundles and amorphous spacings. The blend of the same composition crystallized at 220°C had amorphous ellipsoids of 0.35 μm and failed by cracking through the spherulite without any large-scale deformation. Presumably, a critical particle size of approximately 0.6 μm exists around which development of large compressive stresses in the sPS-rich (more brittle) amorphous domains induces their bulk deformation. Interestingly, the transition of mode of failure from crazing to combination of crazing and shear yielding in PPO and high-impact polystyrene (HIPS) blends also takes place at 50% PPO content.[23]

The tensile properties of the cold crystallized blends, on the other hand, were almost independent of the temperature of crystallization. The SEM micrographs showed that medium size (55–65 nm) lamellar bundles were formed. These lamellar bundles were separated by finer amorphous regions formed after cold crystallization. The dimensions of these bundles and the amorphous domains varied little with the crystallization temperatures (and hence, the crystallization rates). The tensile properties were also practically unchanged at different crystallization temperatures.

CONCLUSIONS

The study shows that semicrystalline polymer blends can crystallize to form spherulitic structures containing crystalline bundles separated by amorphous regions. The texture of these structures depends on composition and processing conditions. In melt-miscible blends, these structures may offer an alternate route to redistribute the noncrystallizable material and control the composition and size of amorphous domains. Moreover, these amorphous domain sizes are critical in achieving better mechanical properties. The incorporation of the loops, chain ends, and interentanglement of the chains may help in preserving the interfacial bond between the phases. In melt-miscible sPS/PPO blends, at 50% PPO content, tensile properties mode of failure varied appreciably with crystallization temperature. The ellipsoid interfibrillar amorphous domains of size 0.6 μm were drawn and the samples gave high tensile strength. No sign of failure along the interfaces of the phases formed after crystallization was observed.

The authors thank Dow Chemical Co. for kindly providing the syndiotactic polystyrene. This research was supported by the DuPont Educational Aid Program.

References

1. Bucknall, C. B. Toughened Plastics; Applied Science Publishers: London, 1977.
2. Michler, G. H. Acta Polym 1985, 36, 285.
3. Wu, S. J Appl Polym Sci 1988, 35, 549.
4. Pearson, R. A.; Yee, A. F. J Mater Sci 1991, 26, 3828.
5. Sue, H.-J.; Yee, A. F. J Mater Sci 1989, 24, 1447.
6. Kambour, R. P. J Polym Sci Macromol Rev 1973, 7, 1.

7. Nair, S. V.; Wong, S.-C.; Goettler, L. A. J Mater Sci 1997, 32, 5347.
8. Evans, A. G.; Williams, S.; Beaumont, P. W. R. J Mater Sci 1985, 20, 3668.
9. Wei, G.-X.; Sue, H.-J.; Chu, J.; Huang, C.; Gong, K. J Mater Sci 2000, 35, 555.
10. Kurauchi, T.; Ohta, T. J Mater Sci 1984, 19, 1699.
11. Koo, K.-K; Inoue, T.; Miyasaka, K. Polym Eng Sci 1985, 25, 741.
12. Heino, M.; Kirjava, J.; Hietaoja, P.; Seppala, J. J Appl Polym Sci 1997, 65, 241.
13. Kit, K. M.; Schultz, J. M. J Polym Sci 1998, 36, 873.
14. Keith, H. D.; Padden, F. J. J Appl Phys 1963, 34, 2409.
15. Keith, H. D.; Padden, F. J. J Appl Phys 1964, 35, 1270.
16. Keith, H. D.; Padden, F. J. J Appl Phys 1964, 35, 1286.
17. Dutt, G.; Kit, K. M. J Appl Polym Sci 2002, 87, 1975.
18. Cimmino, S.; Pace, E. D.; Martuscelli, E.; Silvestre, C. Polymer 1993, 34, 2799.
19. Chu, J.-N.; Schultz, J. M. J Mater Sci 1990, 25, 3746.
20. Donald, A. M.; Kramer, E. J. J Appl Polym Sci 1997, 27, 3729.
21. Majumdar, B.; Keskkula, H.; Paul, D. R. J Polym Sci Part B: Polym Phys 1994, 32, 2127.
22. Wu, S. Polymer 1985, 26, 1855.
23. Bucknall, C. B.; Clayton, D.; Keast, W. E. J Mater Sci 1972, 7, 1443.